

AD-A164 190

A COMPUTATIONAL MODEL FOR CONTACT STRESS PROBLEMS(U)  
VIRGINIA POLYTECHNIC INST AND STATE UNIV BLACKSBURG  
DEPT OF E J N REDDY ET AL JAN 86 VPI-E-86 2

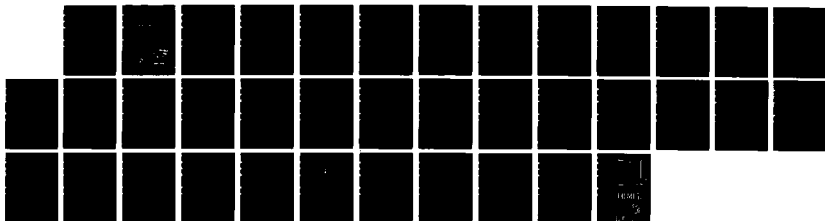
1/1

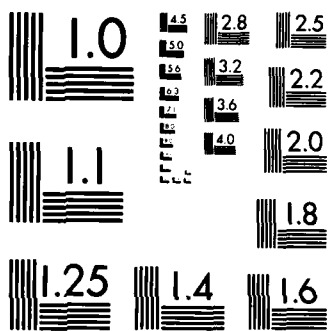
UNCLASSIFIED

N00014-84-K-8552

F/G 28/11

ML





MICROCOPY RESOLUTION TEST CHART  
NBS-1963-A

12

# COLLEGE OF ENGINEERING

AD-A164 190

INTERIM REPORT

Research Report No. VPI-E-86.2

A COMPUTATIONAL MODEL FOR CONTACT STRESS PROBLEMS

by

J. N. Reddy and P. R. Heyliger  
Department of Engineering Science and Mechanics  
Virginia Polytechnic Institute and State University  
Blacksburg, Virginia 24061

DTIC FILE COPY



DTIC  
FEB 12 1986

*ES*

# VIRGINIA POLYTECHNIC INSTITUTE AND STATE UNIVERSITY

BLACKSBURG,  
VIRGINIA

This document is approved for public distribution

86 2 10 119

Department of the Navy  
OFFICE OF NAVAL RESEARCH  
Mechanics Division  
Arlington, Virginia 22217

Contract N00014-84-K-0552  
Project NR 064-727/5-4-84 (430)  
INTERIM REPORT

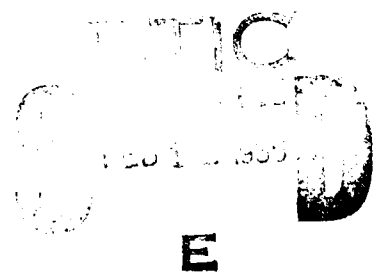
Research Report No. VPI-E-86.2

A COMPUTATIONAL MODEL FOR CONTACT STRESS PROBLEMS

by

J. N. Reddy and P. R. Heyliger  
Department of Engineering Science and Mechanics  
Virginia Polytechnic Institute and State University  
Blacksburg, Virginia 24061

Accession For	
NTIS GRA&I	<input checked="" type="checkbox"/>
DTIC TAB	<input type="checkbox"/>
Unannounced	<input type="checkbox"/>
Justification	
By	
Identification/	
Applicable Codes	
Distribution/for	
Dist	Special
<b>A-1</b>	



January 1986

Approved for public release; distribution unlimited.

## A COMPUTATIONAL MODEL FOR CONTACT STRESS PROBLEMS

J. N. Reddy<sup>‡</sup> and P. R. Heyliger\*  
Department of Engineering Science and Mechanics  
Virginia Polytechnic Institute and State University  
Blacksburg, Virginia 24061

### SUMMARY

A mixed finite element model based on the incremental nonlinear theory of solid bodies is developed and its numerical accuracy is evaluated by applying the model to a number of contact problems. The theoretical basis of the finite element model is formulated using the updated Lagrangian formulation. Both displacement and mixed models are described, but emphasis is placed on the development and application of the mixed model, which contains the displacements and stresses as the nodal degrees of freedom.

### INTRODUCTION

In the linear description of the motion of solid bodies it is assumed that the displacements are infinitely small and that the material is linearly elastic. In addition, it is also assumed that the nature of the boundary conditions remains unchanged during the entire deformation process. These assumptions imply that the displacement vector  $\underline{u}$  is a linear function of the applied load vector  $\underline{F}$ , i.e., if the applied load vector is a scalar multiple  $\alpha \underline{F}$  then the corresponding displacements are  $\alpha \underline{u}$ .

The nonlinearity in solid mechanics arises from two distinct sources. One is due to the kinematics of deformation of the body and

---

<sup>‡</sup>Clifton C. Garvin Professor of Engineering Science and Mechanics.

\*Graduate Research Assistant.

the other from the constitutive behavior (i.e., stress-strain relations). The analyses in which the first type of nonlinearity is considered are called geometrically nonlinear analyses, and those in which the second type are considered are called materially nonlinear analyses. The geometrically nonlinear analysis can be subclassified according to the type of nonlinearities considered. Two such cases are: (i) large displacements, large rotations, but small strains, and (ii) large displacements, large rotations and large strains. In the first case it is assumed that rotations of line elements are large, but their extensions and changes of angles between two line elements are small. In the second case the extension of a line element and angle changes between two line elements are large, and displacements and rotations of a line element are also large.

The objective of the present study is two-fold: First, to describe the equations that govern the nonlinear behavior of solids, and second, to develop finite element models for the analysis of the nonlinear behavior of solid bodies in contact.

#### INCREMENTAL EQUATIONS OF MOTION

Consider the motion of a body in a fixed Cartesian coordinate system. Suppose that the body can experience large displacements, large strains and nonlinear mechanical (i.e. constitutive) behavior. We wish to determine the configuration of the body for different times and loads. The formulation to be described assumes that the configurations of the body,  $c_1, c_2, \dots, c_n$  due to loads  $P_1, P_2, \dots, P_n$ , respectively are known and seeks the configuration at time  $c_{n+1}$ . Thus, in the present formulation we follow the body as it deforms from the initial configuration to the final configuration. This type of

description is called the Lagrangian (or material) description, which differs from the Eulerian description used in fluid mechanics problems. In the Eulerian description of motion, instead of following the body (or a fixed collection of particles constituting the body), the motion of particles passing through a fixed control volume is determined for various times. The Lagrangian description is a natural one for a solid body because one is more interested in the deformation of the body than in the changes that are taking place in the control volume that was occupied initially by the body. On the other hand, the Eulerian description is a natural one for fluid flow problems, because there one is interested in the velocity, pressure and stress fields in a fixed control volume without focusing attention on fluid particles that enter and leave the control volume.

In the Lagrangian description of motion all variables are referred to a reference configuration, which can be the initial configuration or any other convenient configuration. The description in which all variables are referred to the current configuration is called the updated Lagrangian description [1-4] and the one in which all variables are referred to the initial configuration is called the total Lagrangian description [5-8].

The equations of the Lagrangian incremental description of motion can be derived from the principles of virtual work (i.e., virtual displacements, virtual forces or mixed virtual displacements and forces) [9-13]. Since our ultimate objective is to develop the finite element models of the equations governing a body, we will not actually derive the differential equations of motion but utilize the virtual work statements to develop the finite element models.

### Displacement Formulation

The displacement finite element model is based on the principle of virtual displacements (see Reddy [14]). The principle requires that the sum of the external virtual work done on a body and the internal virtual work stored in the body should be equal to zero:

$$\int_{V_2} {}^2\tau_{ij} \delta({}^2e_{ij}) dV - \delta({}^2F) = 0 \quad (1)$$

$$\delta({}^2F) = \int_{V_2} {}^2f_i \delta u_i dV + \int_{S_2} {}^2t_i \delta u_i dS$$

where

${}^2\tau_{ij}$  = the Cartesian components of the Cauchy stress tensor in configuration  $c_2$  at time  $(t + \Delta t)$  occupying the volume  $V_2$

${}^2e_{ij}$  = the Cartesian components of the infinitesimal strain tensor associated with the displacements  $u_i$  in going from configuration  $c_1$  at time  $t$  to  $c_2$  at time  $(t + \Delta t)$  :

$${}^2e_{ij} = \frac{1}{2} \left( \frac{\partial u_i}{\partial x_j} + \frac{\partial u_j}{\partial x_i} \right) \quad (2)$$

$x_i$  = Cartesian components of a point in configuration  $c_2$ .

${}^2f_i$  = Cartesian components of the body force vector measured in  $c_2$

${}^2t_i$  = Cartesian components of the surface stress vector measured in  $c_2$

Here  $\delta$  denotes the variational symbol (i.e.,  $\delta u_i$  denotes the virtual displacement in  $u_i$ ) and  $dV$  and  $dS$  denote the volume and surface elements in the configuration over which the integrals are defined.

Equation (1) is not so useful in its present form because the integrals are defined over the volume  $V_2$  and surface  $S_2$  of the configuration  $c_2$ , which is yet unknown. In the linear analysis, it is assumed that the configuration of the body remains unchanged and therefore Eq. (1) applies to the initial (undeformed) configuration. The fact that the configuration of the body changes continuously in a nonlinear analysis requires us to use appropriate measures of stress and strain and their interrelationship (i.e., constitutive equations) so that Eq. (1) can be used to calculate the configuration  $c_2$ . In order to compute the current configuration  $c_2$  (often, the displacements, strains and stresses in  $c_2$ ) from the knowledge of applied forces and displacements and known previous configurations  $c_1$ , we must make some assumptions. A description of the procedure based on the updated Lagrangian approach is given below.

The coordinates of a general point in  $c_0$  and  $c_1$  and  $c_2$  are denoted by  $(X_1^0, X_2^0, X_3^0)$ ,  $(X_1, X_2, X_3)$ , and  $(x_1, x_2, x_3)$ , respectively. The displacements of a general point in  $c_1$  are denoted by  $({}^1u_1, {}^1u_2, {}^1u_3)$ . In  $c_2$  they are given by

$${}^2u_i = {}^1u_i + u_i, \quad i = 1, 2, 3 \quad (3)$$

where  $u_i$  are the components of the displacement vector from  $c_1$  to  $c_2$ .

During the motion of the body, its volume, surface area, density, stresses and strains change continuously. The stress measure that we shall use is the second Piola-Kirchhoff stress tensor. The components of the second Piola-Kirchhoff stress tensor in  $c_1$  will be denoted by  $S_{ij}$ . To see the meaning of the second Piola-Kirchhoff stress tensor, consider the force  $d\bar{F}$  on surface  $dS$  in  $c_2$ . The Cauchy stress

tensor  $\underline{\tau}$  is defined by

$$(\hat{n} \cdot \underline{\tau}) dS = dF \quad (4a)$$

where  $\hat{n}$  is the unit normal to  $dS$  in  $c_2$ . Note that the Cauchy stress is the force per deformed area (i.e. measured in  $c_2$ ) and referred to  $c_2$ .

The second Piola-Kirchhoff stress tensor at time  $t + \Delta t$  referred to  $c_1$  is defined by

$$(\hat{n}_0 \cdot \underline{{}^2S}) dS_0 = dF_0 \quad (4b)$$

where  $\hat{n}_0$  denotes the unit normal to the surface element  $dS_0$  in  $c_1$ . The force  $dF_0$  is related to  $dF$  by

$$dF_0 = \underline{J}^{-1} \cdot dF \quad (4c)$$

where

$$\underline{J}^{-1} = \left( \frac{\partial X}{\partial x} \right)^T$$

From the definition it is clear that the second Piola-Kirchhoff stress is measured in  $c_2$  but referred to  $c_1$ . It can be shown that (see Malvern [15]) that the components  ${}^2S_{ij}$  and  ${}^2\tau_{ij}$  are related according to

$${}^2S_{ij} = \frac{\rho_0}{\rho} \frac{\partial X_i}{\partial x_m} \cdot {}^2\tau_{mn} \cdot \frac{\partial X_j}{\partial x_n} \quad (5a)$$

$${}^2\tau_{ij} = \frac{\rho}{\rho_0} \frac{\partial x_i}{\partial X_m} \cdot {}^2S_{mn} \cdot \frac{\partial x_j}{\partial X_n} \quad (5b)$$

where  $\rho_0$  denotes the density in  $c_1$  and  $\rho$  is the density in  $c_2$ . The second Piola-Kirchhoff stress tensor is symmetric whenever the Cauchy stress tensor is symmetric. Note that  ${}^2S_{ij} = {}^2\tau_{ij} \equiv {}^2\tau_{ij}$ .

Similarly, the Green-Lagrange strain tensor  $E_{ij}$  and the infinitesimal strain tensor  $e_{ij}$  are related by

$${}^2_1E_{ij} = \frac{\partial x_m}{\partial X_i} \frac{\partial x_n}{\partial X_j} {}^2e_{mn} \quad (6)$$

It is also important to note that the 2nd Piola-Kirchhoff stress tensor is energetically conjugate to the Green-Lagrange strain tensor and the Cauchy stress is energetically conjugate to the infinitesimal strain tensor. In other words, we have

$$\int_{V_1} {}^2_1S_{ij} \delta({}^2_1E_{ij}) dV = \int_{V_2} {}^2\tau_{ij} \delta({}^2e_{ij}) dV \quad (7)$$

Substituting the equality (7) into Eq. (1), we obtain

$$0 = \int_{V_1} {}^2_1S_{ij} \delta({}^2_1E_{ij}) dV - \delta({}^2F) \quad (8)$$

Next we use the incremental decompositions of the stresses and strains:

$$\begin{aligned} {}^2_1S_{ij} &= {}^1\tau_{ij} + {}^1S_{ij} \\ {}^2_1E_{ij} &= {}^1e_{ij} + {}^1n_{ij} \end{aligned} \quad (9)$$

where

$$\begin{aligned} {}^1S_{ij} &= \text{incremental components of 2nd Piola-Kirchhoff stress tensor} \\ {}^1e_{ij} &= \text{(incremental) components of the infinitesimal strain tensor} \\ &= \frac{1}{2} \left( \frac{\partial u_i}{\partial X_j} + \frac{\partial u_j}{\partial X_i} \right), \\ {}^1n_{ij} &= \frac{1}{2} \frac{\partial u_m}{\partial X_i} \frac{\partial u_m}{\partial X_j} \end{aligned} \quad (10)$$

Recall that  $u_i$  is the  $i$ -th displacement component of a generic point in  $c_1$  (in going from  $c_1$  to  $c_2$ ). Substituting Eq. (9) into Eq. (8), we have

$$0 = \int_{V_1} ({}^1\tau_{ij} + {}^1S_{ij}) \delta({}_1e_{ij} + {}_1n_{ij}) dv - \delta({}^2F) .$$

or

$$\begin{aligned} \int_{V_1} {}^1S_{ij} \delta({}_1e_{ij} + {}_1n_{ij}) dv + \int_{V_1} {}^1\tau_{ij} \delta({}_1n_{ij}) dv \\ = - \int_{V_1} {}^1\tau_{ij} \delta({}_1e_{ij}) dv + \delta({}^2F) \end{aligned} \quad (11)$$

Linearize the equations by assuming that

$${}^1S_{ij} = {}^1C_{ijrs} e_{rs}, \quad \delta {}^2E_{ij} = \delta {}_1e_{ij} \quad (12)$$

We obtain the approximate equation of equilibrium,

$$\begin{aligned} \int_{V_1} {}^1C_{ijrs} {}^1e_{rs} \delta({}_1e_{ij}) dv + \int_{V_1} {}^1\tau_{ij} \delta({}_1n_{ij}) dv \\ = - \int_{V_1} {}^1\tau_{ij} \delta({}_1e_{ij}) dv + \delta({}^2F) \end{aligned} \quad (13)$$

This linearization can be interpreted as a representation of the nonlinear curve between two consecutive load steps by a linear line segment.

### Mixed Formulation

A mixed (or stationary) virtual work statement that treats the displacements and stresses as independent (dependent) variables can be derived from Eq. (13) as follows. First, we note that Eq. (13) is the first variation of the functional

$$\pi = \int_{V_1} \frac{1}{2} {}^1C_{ijrs} {}^1e_{rs} {}^1e_{ij} dv + \int_{V_1} {}^1\tau_{ij} ({}_1e_{ij} + {}_1n_{ij}) dv - {}^2F \quad (14)$$

Clearly,  $\pi$  denotes the (approximate) total potential energy of the body in configuration  $c_2$  but referred to configuration  $c_1$ , and Eq. (13) is a

statement of the principle of the minimum total potential energy. In Eqs. (13) and (14) it is understood that  ${}^1e_{ij}$  and  ${}^1n_{ij}$  are defined in terms of  $u_j$  [see Eq. (10)].

In the mixed formulation, we begin with the expression for the approximate total potential energy  $\pi$  and introduce the stresses as variables using the Lagrange multiplier method. We treat the strain-displacement relations

$${}^1e_{ij} = \frac{1}{2} \left( \frac{\partial u_i}{\partial x_j} + \frac{\partial u_j}{\partial x_i} \right) \quad (15)$$

as constraints and let the increment in the 2nd Piola-Kirchhoff stress tensor  ${}^1S^{ij}$  act as the Lagrange multiplier. Including this in the variational form results in the modified functional  $\pi_L$ , which is given by

$$\pi_L = \pi - \int_{V_1} {}^1S_{ij} \left[ {}^1e_{ij} - \frac{1}{2} \left( \frac{\partial u_i}{\partial x_j} + \frac{\partial u_j}{\partial x_i} \right) \right] dV \quad (16)$$

where  $\pi$  is given by Eq. (14). Here we note that the sign of the Lagrange multiplier term is generally arbitrary, and is selected as negative to obtain the correct form of the equations that follow.

The variational principle (often called the Hellinger-Reissner variational principle) is given by setting  $\delta\pi_L = 0$ . This gives

$$\begin{aligned} \delta\pi_R = \int_{V_1} \{ & {}^1\tau_{ij} \delta {}^1e_{ij} + {}^1\tau_{ij} \delta {}^1n_{ij} + \delta \left( \frac{1}{2} C_{ijkl} {}^1e_{ij} {}^1e_{kl} - {}^1S_{ij} {}^1e_{ij} \right) \\ & + \delta {}^1S_{ij} u_{i,j} + {}^1S_{ij} \delta u_{i,j} \} dV - \delta({}^2F) = 0 \end{aligned} \quad (17)$$

We next write the expressions for the strain energy density  $U_0$  and the complementary strain energy density  $U_0^*$  due to the incremental displacements as

displacements as

$$U_0 = \frac{1}{2} C_{ijkl} \epsilon_{ij} \epsilon_{kl} \quad (18)$$

and

$$U_0^* = \frac{1}{2} D_{ijkl} S_{ij} S_{kl}$$

where  $D_{ijkl}$  are the components of the compliance tensor. We may then write

$$- U_0^* = U_0 - \epsilon_{ij} \epsilon_{ij} \quad (19)$$

and, taking the variation of this expression gives

$$- \delta U_0^* = \delta \left( \frac{1}{2} C_{ijkl} \epsilon_{ij} \epsilon_{kl} - \epsilon_{ij} \epsilon_{ij} \right) \quad (20)$$

If we write the complementary strain energy density in terms of the 2nd Piola-Kirchhoff stress components as we did in Eq. (18) we may write

$$- \delta U_0^* = - \frac{\partial U_0^*}{\partial S_{ij}} \delta S_{ij} = - D_{ijkl} S_{kl} \delta S_{ij} \quad (21)$$

Equating the expressions in Eqs. (20) and (21) and substituting into Eq. (17) yields the two approximate equilibrium equations

$$\int_{V_1} \tau_{ij} \delta(\epsilon_{ij}) dV + \int_{V_1} S_{ij} \delta u_{i,j} dV = \delta(2F) - \int_{V_1} \tau_{ij} \delta(\epsilon_{ij}) dV \quad (22)$$

$$\int_{V_1} u_{i,j} \delta(S_{ij}) dV - \int_{V_1} D_{ijkl} S_{kl} \delta(S_{ij}) dV = 0$$

These two equations are analogous to Eq. (13) for the displacement formulation.

In the next section we discuss the finite element models of Eqs. (13) and (22).

## FINITE ELEMENT MODELS

### Displacement Model

Here we construct the finite element model of Eq. (13) for the two-dimensional case. We assume that the displacement components are interpolated by expressions of the form (see Reddy [16])

$$u_i(x_1, x_2) = \sum_{j=1}^n u_i^j \psi_j(x_1, x_2) \quad (23)$$

where  $u_i^j$  denote the value of  $u_i$  at the  $j$ -th node, and  $\psi_j$  denote the interpolation functions. Substituting Eq. (23) into Eq. (13) we obtain

$$([K^L] + [K^\sigma]) \{\Delta\} = \{F^L\} - \{F^\sigma\} \quad (24)$$

where

$$[K^L] = t \int_{A_1} [B^L]^T [C] [B^L] dA, \quad t = \text{thickness}$$

$$[C] = \begin{bmatrix} C_{11} & C_{12} & C_{16} \\ C_{12} & C_{22} & C_{26} \\ C_{16} & C_{26} & C_{66} \end{bmatrix},$$

$$[B^L]_{(3 \times 2n)} = \begin{bmatrix} \psi_{1,1} & 0 & \psi_{2,1} & 0 & \dots & \psi_{n,1} & 0 \\ 0 & \psi_{1,2} & 0 & \psi_{2,2} & \dots & 0 & \psi_{n,2} \\ \psi_{1,2} & \psi_{1,1} & \psi_{2,2} & \psi_{2,1} & \dots & \psi_{n,2} & \psi_{n,1} \end{bmatrix}$$

$$[K^\sigma] = t \int_{A_1} [B^\sigma]^T [\tau] [B^\sigma] dA$$

$$[B^\sigma]_{(4 \times 2n)} = \begin{bmatrix} \psi_{1,1} & 0 & \psi_{2,1} & 0 & \dots & \psi_{n,1} & 0 \\ \psi_{1,2} & 0 & \psi_{2,2} & 0 & \dots & \psi_{n,2} & 0 \\ 0 & \psi_{1,1} & 0 & \psi_{2,1} & \dots & 0 & \psi_{n,1} \\ 0 & \psi_{1,2} & 0 & \psi_{2,2} & \dots & 0 & \psi_{n,2} \end{bmatrix}$$

$$[\tau] = \begin{bmatrix} \tau_{11} & \tau_{12} & 0 & 0 \\ \tau_{12} & \tau_{22} & 0 & 0 \\ 0 & 0 & \tau_{11} & \tau_{12} \\ 0 & 0 & \tau_{12} & \tau_{22} \end{bmatrix}$$

$$\{F^L\} = t \int_{A_1} [\psi]^T \{f\} dA, \quad \{F^o\} = t \int_{A_1} [B^L]^T \{\tau\} dA$$

$$\begin{matrix} [\psi] \\ (2 \times 2n) \end{matrix} = \begin{bmatrix} \psi_1 & 0 & \psi_2 & 0 & \dots & \psi_n & 0 \\ 0 & \psi_1 & 0 & \psi_2 & \dots & 0 & \psi_n \end{bmatrix}, \quad \{\tau\} = \begin{Bmatrix} \tau_{11} \\ \tau_{22} \\ \tau_{12} \end{Bmatrix}, \quad \{f\} = \begin{Bmatrix} f_1 \\ f_2 \end{Bmatrix} \quad (25)$$

It is understood that  ${}^1\tau_{ij}$  is computed using the Almansi strain tensor,

$${}^1\tau_{ij} = {}^1C_{ijkl} {}^1\epsilon_{km} \quad (26)$$

$${}^1\epsilon_{km} = \frac{1}{2} \left( \frac{\partial u_j}{\partial X_m} + \frac{\partial u_m}{\partial X_k} - \frac{\partial u_m}{\partial X_k} \frac{\partial u_m}{\partial X_m} \right)$$

where the displacements are now the total displacement components measured in the current configuration. Also, since Eq. (13) is a linearized version of Eq. (11), the error introduced into the calculation of the displacements  $u_i$  between configurations can drift the solution away from the true solution (especially if the load steps are large). Therefore, a correction should be made to the displacements at each load step. This can be done as follows: The solution  $\{\Delta\}$  of Eq. (24) allows us [with the aid of Eq. (23)] to compute the total displacements at time  $(t + \Delta t)$ ,

$${}^2u_i = {}^1u_i + u_i$$

which can be used to compute the strains and stresses (with appropriate constitutive equation) at time  $t + \Delta t$ . By the principle of virtual displacements, the true displacements, strains and stresses at any time, say at time  $t + \Delta t$ , are such that the internal virtual work is equal to the external virtual work done. Since  $u_i$  (hence the strains and stresses computed from them) are approximations, there will be an imbalance between the internal and external virtual works performed on the body. This imbalance can be minimized by updating the internal virtual work through an iteration (for a fixed system of loads and time); the iteration is continued until the imbalance is reduced to a preassigned value (i.e., a convergence limit). For example, the displacement increment at the  $(r + 1)$ st iteration is calculated from the equations

$$([K^L] + [K^\sigma])_r \{\Delta\}_{r+1} = \{F^L\} - \{F^\sigma\}_r \quad (27)$$

wherein  $[\tau]$  and  $\{\tau\}$  are calculated using the displacements,

$$({}^2u_i)_r = ({}^2u_i)_{r-1} + (u_i)_r \quad (20)$$

Equations (27) and (28) correspond to the Newton-Raphson iteration. If the left hand side is not updated during the iteration, the iterative scheme is known as the modified Newton-Raphson iteration.

### Mixed Model

We next construct the finite element model of Eqs. (22) for the two-dimensional case. We begin by assuming independent approximations of the displacements and stresses of the form

$$u_i(x_1, x_2) = \sum_{j=1}^n u_i^j \psi_j(x_1, x_2) \quad (29)$$

$${}_1S_{ij}(x_1, x_2) = \sum_{k=1}^n {}_1S_{ij}^k \psi_k(x_1, x_2)$$

Substituting these expressions into the two equilibrium equations in Eq. (22) gives

$$\begin{bmatrix} [K^{11}] & [K^{12}] \\ [K^{12}]^T & [K^{22}] \end{bmatrix} \begin{Bmatrix} \{u\} \\ \{s\} \end{Bmatrix} = \begin{Bmatrix} \{F^L\} \\ \{0\} \end{Bmatrix} - \begin{Bmatrix} \{F^{NL}\} \\ \{0\} \end{Bmatrix} \quad (30)$$

where

$$[K^{11}] = t \int_{A_1} [B^\sigma]^T [\tau] [B^\sigma] dA$$

$$[K^{22}] = t \int_{A_1} [\psi^\sigma]^T [D] [\psi^\sigma] dA$$

$$[K^{12}] = t \int_{A_1} [B^L]^T [\psi^\sigma] dA \quad (31)$$

$$\{F^L\} = t \int_{A_1} [\psi]^T \{f\} dA$$

$$\{F^{NL}\} = t \int_{A_1} [B^L]^T \{\tau\} dA$$

$${}_{(3 \times 3n)} [\psi^\sigma] = \begin{bmatrix} \psi_1 & 0 & 0 & \psi_2 & 0 & 0 & \dots & \psi_n & 0 & 0 \\ 0 & \psi_1 & 0 & 0 & \psi_2 & 0 & \dots & 0 & \psi_n & 0 \\ 0 & 0 & \psi_1 & 0 & 0 & \psi_2 & \dots & 0 & 0 & \psi_n \end{bmatrix}$$

$$[D] = \begin{bmatrix} D_{11} & D_{12} & D_{16} \\ D_{12} & D_{22} & D_{26} \\ D_{16} & D_{26} & D_{66} \end{bmatrix} \quad (32)$$

All of the other necessary matrices have been defined previously during the development of the displacement finite element model.

As with the displacement model, Eq. (30) is solved repeatedly until the force imbalance is reduced to a fixed tolerance. This amounts to measuring the percentage of the displacement and stress increments relative to the total solution vector. When the increase in the displacements and stresses has been reduced to below a very small percentage of the total solution, the state of equilibrium has been obtained for the given load step, and the load may be increased or the analysis may be terminated.

The solution of Eq. (30) allows us to compute the total displacements and Cauchy stresses at time  $(t + \Delta t)$ . To compute the displacements we simply use the equation

$${}^2u_i = {}^1u_i + u_i$$

In the mixed formulation, there is no need to compute the Cauchy stresses using the Almansi strains as was required using the displacement formulation. Since the increments of the 2nd Piola-Kirchhoff stress tensor are computed as nodal variables, we simply use our incremental decomposition of the stress given in Eq. (9) as

$${}^2S_{ij} = {}^1\tau_{ij} + {}^1S_{ij}$$

When the increment in the  ${}^1S_{ij}$  terms is reduced to be within the required tolerance, we have  ${}^2S_{ij} = {}^2\tau_{ij}$ .

#### PLANAR ELASTIC CONTACT PROBLEMS

In this section we discuss several techniques for the analysis of two-dimensional elastic contact problems. Such problems have a host of computational difficulties since the region of contact is typically not known in advance, nor are the regions of relative stick and slip between

the two contacting bodies due to the presence of friction. Most current algorithms that solve contact problems are relatively complex, and use a number of iterative schemes to account for the changing boundary conditions and regions of contact.

The nonlinear mixed finite element formulation forms the cornerstone of the methods described below. The displacement finite element method has been used almost exclusively in previous numerical analyses of contact problems. Mixed elements provide the immediate advantage of computation of stresses as nodal variables, which is ideal for contact problems since the stresses may be obtained precisely on the contact boundary.

Two different and independent methods are described for the analysis of the specific problem of a pin-loaded plate. The methods are described below and several examples are presented for the first of the two techniques.

#### Rigid Pin Contact Algorithm

In general, contact problems involve two or more elastic bodies pressing against one another under external load. In the case of a pin-loaded plate, these two bodies are the plate and the pin. If the assumption of a rigid pin is used, the analysis is simplified considerably. This assumption eliminates the need to analyze the pin, which not only provides a known point of reference for the ensuing contact (i.e. the surface of the pin), but also drastically reduces the resulting global finite element system of equations since there is no need to discretize the domain of the pin.

The assumption of a rigid pin is reasonable if the modulus of elasticity of the pin is much higher than that of the plate. Analytical

studies have also shown that, in the contact analysis of composite plates, pin elasticity is not an important variable and has a relatively small effect on the resulting stress distributions [17].

One simple and effective method for analyzing thin, orthotropic, pin-loaded plates was developed originally by Wilkenson [18] and was later refined by Rahman [19] to capitalize on the computational advantages that arise from the rigid pin assumption. The method uses three separate iteration steps to account for the incremental load level, the contact process, and the effects of friction. Both the original and refined schemes used displacement finite elements. In the load step iteration, the solution for a given load increment was treated as a linear analysis, i.e. the equations of linear elasticity were used. The stresses in the plate were computed, for a given load level, using the original, undeformed configuration of the plate along with the final displacement vector.

The use of displacement elements in the analysis of contact problems frequently results in very large displacement gradients at the region of contact. Since the required stresses are computed at the element interiors and are then extrapolated to the contact boundary, some type of stress smoothing is often necessary using, for example, a local least squares routine [20] or iterative improvement on the averaged nodal stresses [21]. Using mixed elements, this is not necessary since the stresses are computed as nodal variables and no postcomputation is necessary to modify the resulting nodal stresses. It is for this reason that mixed elements would appear to be advantageous over displacement elements for contact problems.

The refined algorithm developed by Rahman [19] uses a mixed polar-Cartesian coordinate system to fix the proper displacements of the nodes of the plate that have come in contact with the pin. An iterative scheme is used to ensure that, for a given load step, all nodes that have come in contact remain in contact. In other words, after every iteration the positions of all contact nodes are corrected in the radial direction so that they remain on the surface of the pin. If the resulting shearing stress for a given contact node is larger than the induced radial stress multiplied by the nodal coefficient of friction, the node is considered to be sliding, and it may subsequently move in the tangential direction of the pin. Otherwise, the node is considered to be sticking to the pin due to friction, and is fixed to an interpolated position on the pin for the remainder of the analysis. This iterative procedure is repeated until the sum of the load steps has reached the required load level. The details of this method are more completely described in reference [19].

#### Elastic Pin Contact Algorithm

The assumption of a rigid pin, which is reasonable for cases when the two bodies in contact have a very large difference in modulus of elasticity, is not usually valid for contact between two generic bodies. The algorithm described in the previous section, though useful for certain problems, was mainly developed to demonstrate the use and accuracy of the mixed finite element method for the analysis of contact problems. For general problems involving arbitrary bodies, it is necessary to revise the analysis to include the effects of pin elasticity, which may be significant if the two bodies are of similar constitution.

To handle the complications arising from contact and the presence of friction between two elastic bodies, we add a Lagrange multiplier contribution to our original expression in Eq. (16), which will represent the total potential of the contact forces acting at the nodes on the contact boundary. In addition, the kinematics of the elements at the contact interface must be monitored such that the nodal displacements are compatible. We therefore invoke stationarity of the modified functional

$$\pi_N = \pi_L - \sum_{i=1}^k W_i$$

where  $k$  represents the number of the contactor nodes on the boundary and  $W$  represents the total potential for a given contact force acting at a given contact node.

Taking the first variation of the modified functional  $\pi_N$  results in a system of equations similar to Eq. (30) with the increment in the contact forces added as new nodal variables for the contactor nodes. These constraint equations may be added to the original stiffness matrices by means of contact matrices, which contain the needed relationships between the contact forces and the contact node displacements. This idea was originated and developed using a displacement formulation by Bathe and Chaudhary [22].

The analysis proceeds in a manner similar to the steps performed for nonlinear solid mechanics problems in that load increments are applied to the body or bodies and the equilibrium equations are solved iteratively until the solution increment is within a preassigned tolerance. If, however, there is penetration of a contactor node from one of the bodies into the domain of a contact element from the other

body during a given iteration, the contact matrices are imposed for the next iteration and the new set of equations is solved until the overlap distance created during the penetration is eliminated. This results in an increase of the contact forces for the nodes involved in the contact as well as a change in the nodal displacements and stresses for these nodes. Inherent in the contact matrices are allowances for stick and slip, and their implementation is a function of the contact stresses and coefficients of friction between the two bodies. The coding of this method is underway and no example problems have been completed to include in this report.

#### HYBRID EXPERIMENTAL/NUMERICAL TECHNIQUE

The primary difficulty in the analysis of contact problems is the lack of knowledge regarding the region of contact and the state of stick or slip between the two bodies. If the regions of contact and the state of stick or slip are known for a given load level, the analysis is greatly simplified. A hybrid experimental/numerical technique has been proposed as part of this research project that combines the experimental technique of moire interferometry with the numerical finite element method to form a hybrid technique. The new method uses the advantages of each of the methods to create an accurate and powerful tool of analysis.

Moire interfereometry provides the required sensitivity that is needed to accurately measure the small in-plane displacements of the two-dimensional pin-loaded plate contact problem. In particular, this method provides valuable information on the state of the displacements at the interface boundary between the pin and the plate. This eliminates the need for any theoretical assumption on exactly what is

occurring at the contact boundary that is so common in most numerical simulations. As mentioned previously, it is the complex state of contact, stick, and slip that makes this problem so difficult to model in a strictly numerical method, and the use of an experimental technique greatly simplifies the computational effort.

The exact displacements of a physical specimen may be measured for a sequence of increasing load steps. These displacement increments, along with the loads applied to the plate, are input as a sequence of nonhomogeneous boundary conditions for the simulated problem analyzed by the nonlinear mixed finite element method. The resulting normal and shearing stresses around the hole of the plate may then be computed to determine the quantitative behavior of the coefficients of friction as a function of the angular position around the hole and the load level. The only approximations introduced are due to the physical and mathematical limitations of moire interferometry and the finite element method. The numerically solved problem is simply a special boundary value problem with specified displacements, and no other assumptions are involved.

Since, in theory, the one half of the plate acts as the mirror image of the other half of the plate, only one half of the plate domain is modeled for the finite element analysis. This also drastically reduces the computational time involved. Preliminary experimental data have shown that the displacements around the hole of the plate are not quite symmetric, even for an isotropic material. This is most probably due to the limitations of creating a perfectly symmetric specimen and applying a perfectly symmetric load. The displacements are therefore averaged in both of the coordinate directions of the plate to yield one

value for a given point of the contact boundary for the modeled half of the plate.

The finite element portion of the analysis currently awaits the reduction of the experimental data for a series of increasing load steps. No examples of the hybrid procedure are included in this report.

### NUMERICAL EXAMPLES

In this section we consider a specific example to demonstrate the characteristics and differences of the displacement and mixed finite element models in nonlinear analysis.

Before considering the example problem, we note an important point on the order of approximation using the mixed elements. Using the results of an eigenvalue analysis of the mixed finite element matrices, Mirza and Olsen [23] proposed and verified a completeness criterion that restricts the choice of the order of approximation for the displacements and stresses. The completeness criterion was given as:

The strains from the stress approximations should possess at least all the strain modes that are present in the strains derived from the displacement approximations.

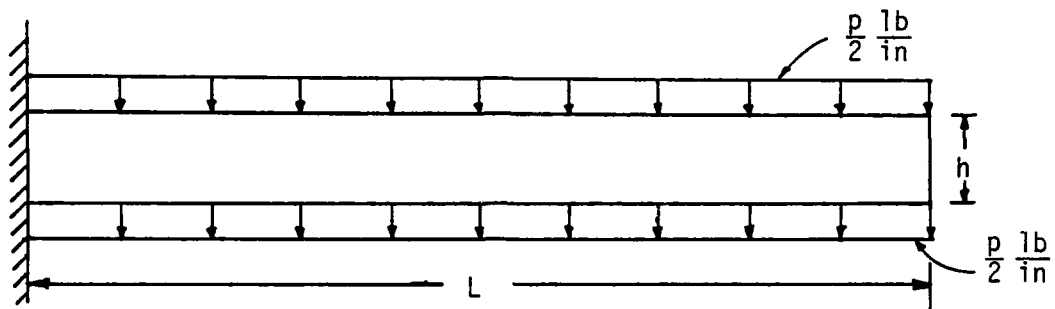
When this criterion is violated, the global stiffness matrix in the mixed model will be singular even after the imposition of the boundary conditions. Isoparametric rectangular elements are used for all of the examples considered herein and, to meet the requirements of the completeness criterion, only linear-linear or quadratic-quadratic combinations are used to approximate the distributions of displacements and stresses in the mixed model. All of the computations were carried out on an IBM 3081 in double precision arithmetic.

### Bending of a Cantilever Beam

The cantilever beam shown in Figure 1 was analyzed using 5 8-node quadratic-quadratic elements using the assumptions of plane stress. The material properties and geometry used are given in the figure. The analysis was completed using 16 equal load steps and a tolerance of  $\epsilon = 0.001$ . The displacements along the line  $x = 0.0$  were specified to be zero.

Figure 2 contains the plot of nondimensionalized tip displacement vs. applied load for the linear analysis and nonlinear analysis as computed by the mixed and displacement finite element models. The mixed model gives displacements that are larger than those of the displacement model, with a maximum difference of 2.8 percent measured at the final load level. Although the results of the displacement model are in excellent agreement with the analytical solution reported by Holden [24], it should be mentioned that Holden's solution uses the Euler-Bernoulli beam theory (i.e., does not even account for the transverse shear strain). However, for a beam of the dimensions used in this example, the shear deformation effect is undoubtedly quite small, and it remains that the mixed element model yields slightly larger displacements than does the displacement model for this example.

It is also of interest to compare the Cauchy stresses determined from the two formulations. In the displacement model, it is necessary to compute the Almansi strain tensor, and then use the constitutive relations of the material, as described in Eq. (26). In the mixed model, we may simply interpolate the values of the nodal stresses using



$L = 10 \text{ in}$

$E = 1.2 \times 10^4 \text{ lb/in}^2$

$h = 1 \text{ in}$

$\nu = 0.2$

Thickness,  $t = 1 \text{ in}$ .

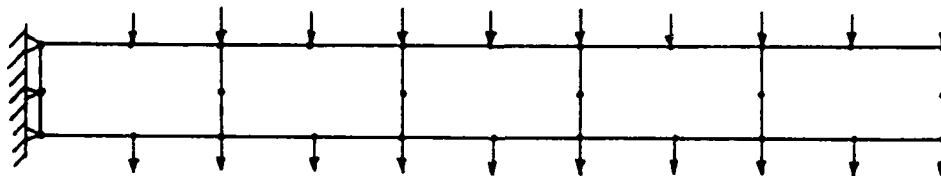


Figure 1 Geometry, material properties, and finite element mesh used for uniformly loaded cantilever beam example.

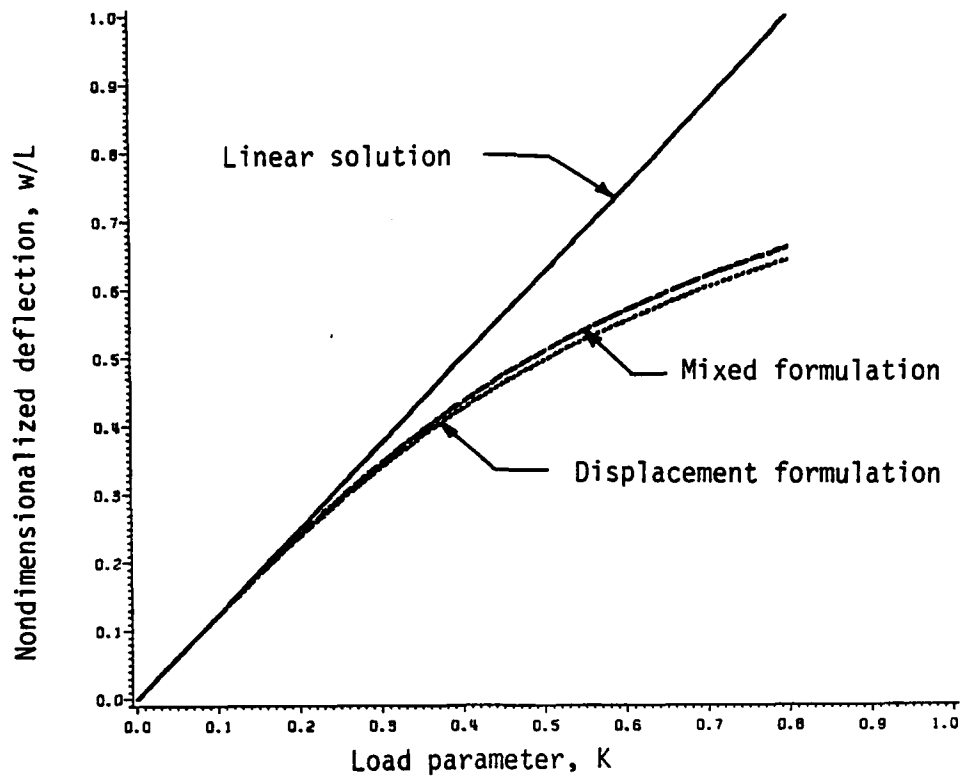


Figure 2 Tip displacement of uniformly loaded cantilever ( $K = PL^3/EI$ )

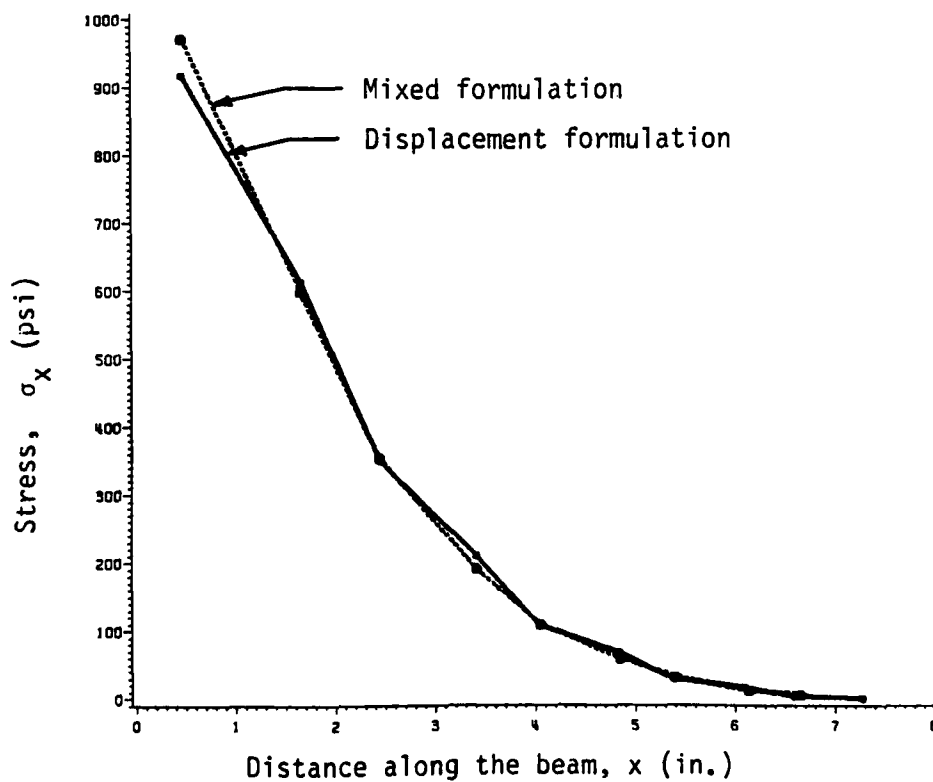


Figure 3 Bending stress along upper Gauss points of cantilever beam

the original form of the stress approximation, i.e.

$$\tau_{ij}(x_1, x_2) = \sum_{k=1}^n \tau_{ij}^k \psi_k(x_1, x_2)$$

To compare the Cauchy stresses using the two formulations, we computed the axial stress  $\tau_{xx}$  at the location of the 2x2 Gauss points along the upper half of the beam. The displacement components from the two models are not exactly the same (the actual positions of the Gauss points vary somewhat), but this difference is very small. The comparison of the axial stress components is shown in Figure 3 for the two different models at the final load level. The agreement is excellent, with the mixed results giving a maximum stress that is 4.8 percent higher than the maximum stress computed using the displacement model. All other computed values are in much closer agreement for the two models.

Although the displacements in the y-direction are in very good agreement for the two formulations, the difference in the displacement gradients can be quite large and can result in significant errors when computing the Cauchy stresses from the Almansi strains using the displacements from the mixed formulation. For example, considering the lower left Gauss point of the rightmost element, we have the following values at a given load step:

	Displacement Formulation	Mixed Formulation
$u_{,x}$	0.003	0.007
$u_{,y}$	0.082	0.082
$v_{,x}$	-0.082	-0.082
$v_{,y}$	0.003	0.007
$\tau_{xx}$	-1.95	51.20

The stress computed from the displacement model is in very good agreement with the stress computed from the mixed model using nodal

stress interpolation, but the stress computed from the Almansi strains using the displacements from the mixed model is very much in error. It appears from the results of this example that the nodal displacements of the mixed model should not be used at any point of the analysis to compute the Cauchy stress components, and the nodal stress values should be used instead.

### Rigid Pin Examples

The contact algorithm proposed by Wilkenson and Rahman was implemented using the three basic iterations of load, contact, and friction using a geometrically nonlinear formulation along with mixed finite elements. Here the results of several example problems involving contact between an elastic body and a rigid pin are presented not only to demonstrate the accuracy of the algorithm but also to highlight the effectiveness of having stress as a nodal variable. The results of the example problems are compared with available analytical and numerical solutions.

In the first example we consider an infinitely long cylinder of radius  $r = 1$  resting on a rigid plane and under a uniform line load. This problem was modeled using the assumptions of plane strain. One quarter of the circular domain was used to model the problem, and was approximated by 84 linear-linear elements. The load was assumed to act at the center of the cylinder and was applied in 12 increments, with the initial increments smaller than the later increments. The problem was modeled by assuming that the cylinder was in contact with a rigid pin of very large radius ( $R = 1000$ ) to model the rigid plane. A tolerance of  $\epsilon = 0.001$  was used for the equilibrium iterations. The modulus of elasticity used was 21,000 ksi and the Poisson's ratio used was 0.3.

The results of the analysis are shown in Figures 4 and 5. The numerical results are compared with the Hertz analytical solution. Figure 4 shows the contact pressure distribution plotted against the distance from the original point of contact. Figure 5 shows the load plotted against the total contact area, the data points of which can only be determined when each successive node comes in contact with the pin. The results from the contact algorithm appear to be quite good.

The second example considers a thin, orthotropic, pin loaded plate with a hole of radius  $r$  under a uniform, in-plane load as shown in Figure 6. Due to symmetry, one half of the plate was modeled using 124 linear-linear elements with 156 nodes for a total of 780 degrees of freedom. The material properties given in the figure are averaged properties from a number of species of wood. The pin was assumed to be rigid and of radius  $R$ . The plate was loaded to a final load of 400 pounds per inch of plate thickness, and was applied in 18 increments. A coefficient of friction of 0.7 was assumed at all points of contact between the plate and the pin for all load levels, and is a typical value for wood on steel. No equilibrium iterations were performed for this problem.

Figure 7 shows the radial stress distribution as a function of the angular position around the pin for the nodes that have come in contact at the final load step. These results are compared with the results obtained by Wilkenson [18] using a finer mesh (385 nodes) and quadratic displacement elements. The comparison is very good.

#### *Acknowledgment*

The support of this work by the Mechanics Division of the Office of Naval Research is gratefully acknowledged. The authors are thankful to Dr. Alan Kusner for the encouragement and support of this work.

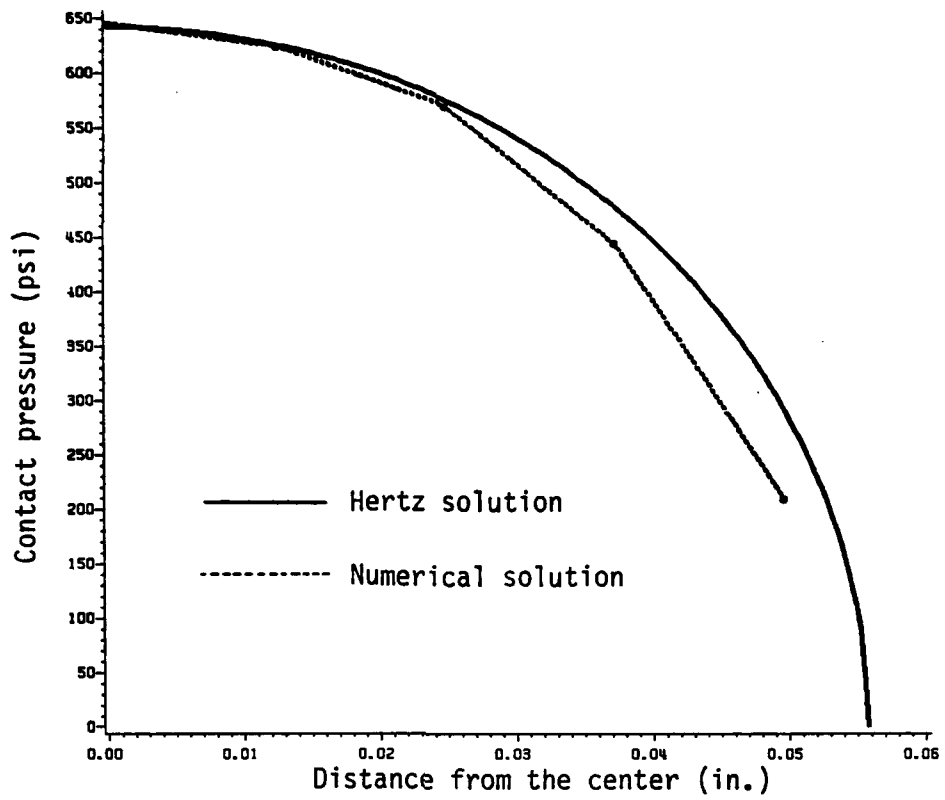


Figure 4 Contact pressure for loaded cylinder

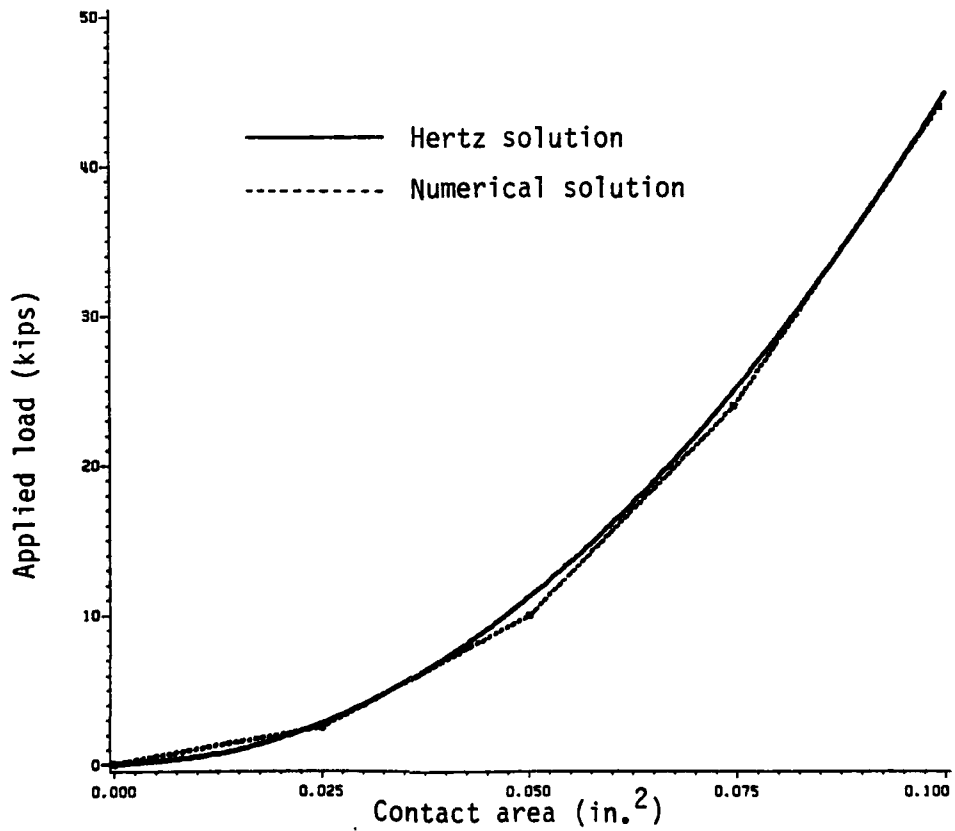


Figure 5 Contact area for loaded cylinder

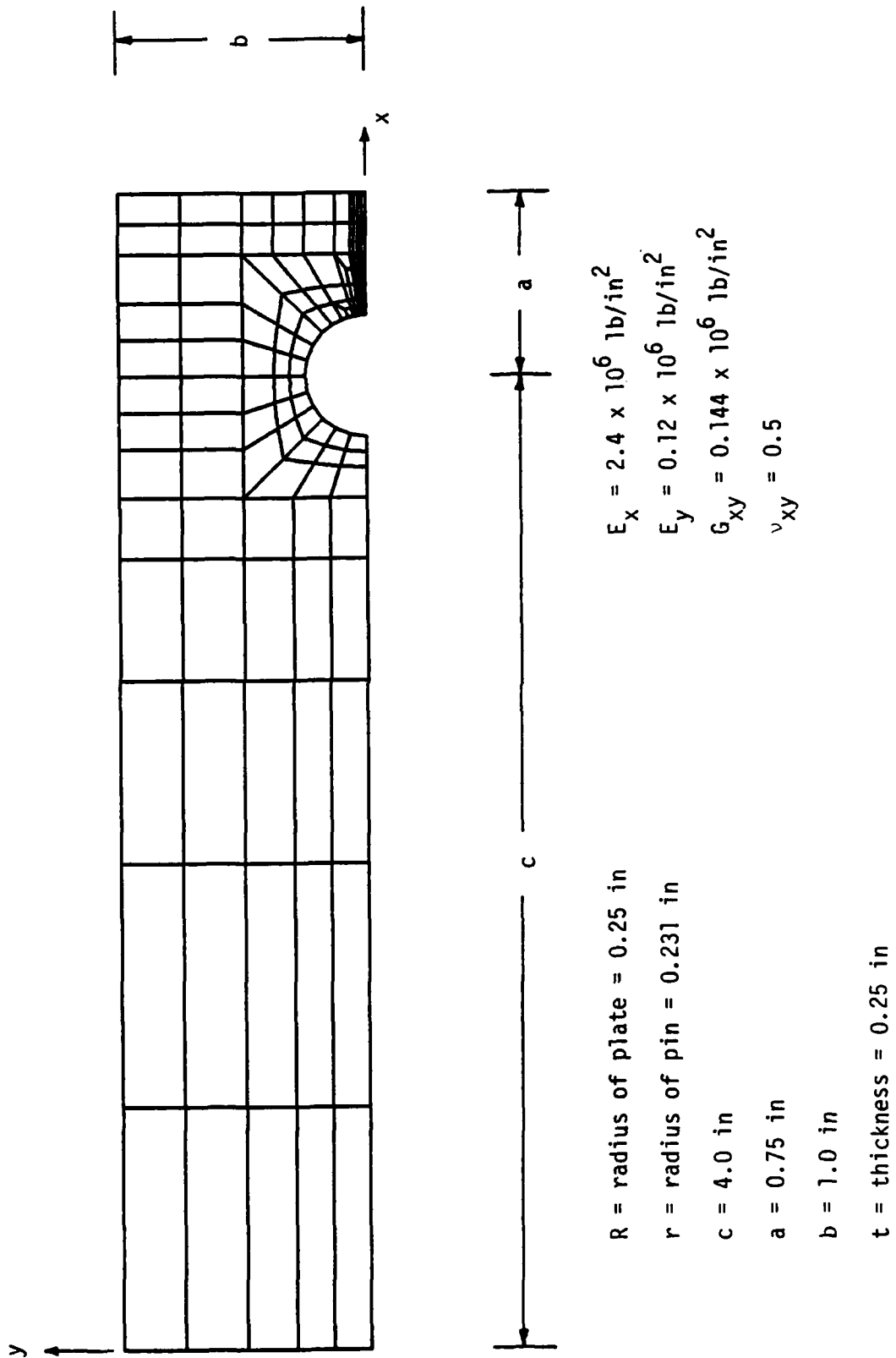


Figure 6 Finite element mesh and material properties for pin-loaded plate example

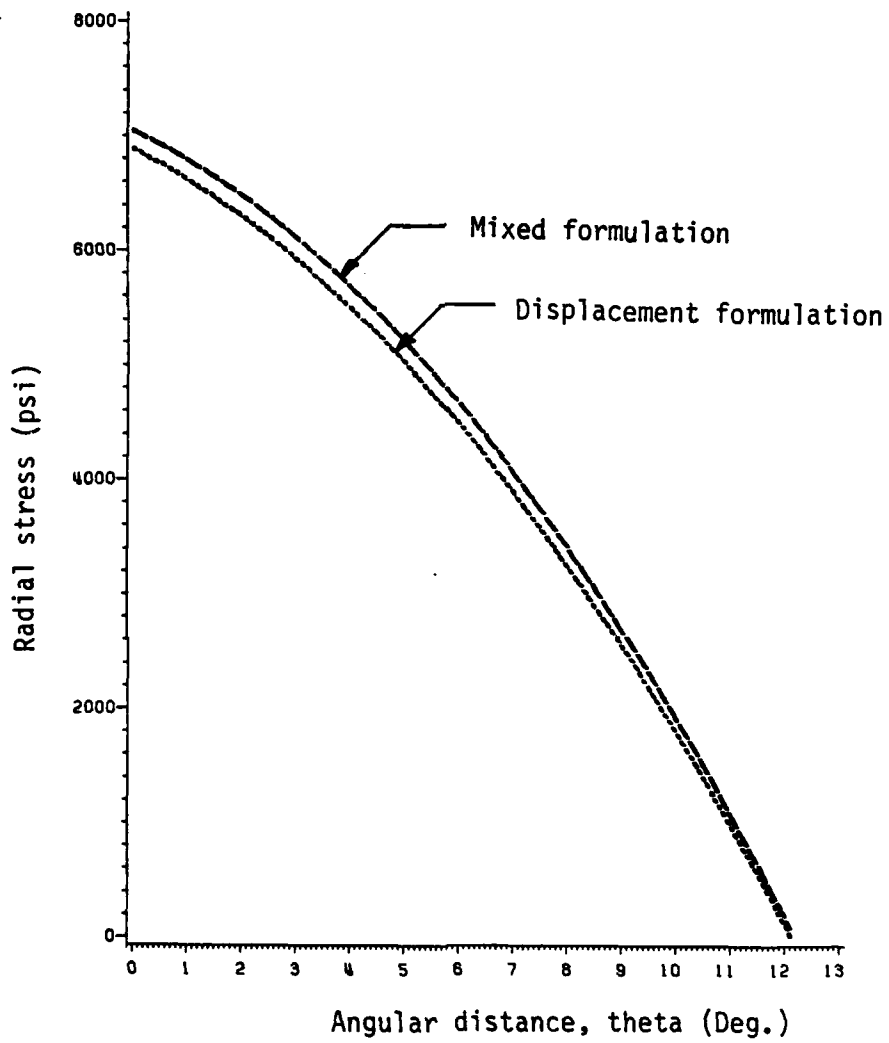


Figure 7 Radial stress around hole of wood plate

## REFERENCES

1. D. W. Murray and E. L. Wilson, "Finite element large deflection analysis of plates," J. Engrg. Mech. Div., ASCE, Vol. 94, pp. 143-165, 1965.
2. S. Yaghai and E. P. Popov, "Incremental analysis of large deflections of shells of revolution," Int. J. Solids Struct., Vol. 7, pp. 1375-1393, 1971.
3. J. A. Stricklin, W. A. Von Riesenmann, J. R. Tillerson and W. E. Haisler, "Static geometric and material nonlinear analysis," Adv. in Comp. Meth. in Struct. Mech. and Design, J. T. Oden, R. W. Clough and Y. Yamamoto (eds.), Univ. of Alabama in Huntsville, pp. 301-324, 1972.
4. Y. Yamada, "Incremental formulations for problems with geometric and material nonlinearities," Adv. in Comp. Meth. in Struct. Mech. and Design, J. T. Oden, R. W. Clough and Y. Yamamoto (eds.), Univ. of Alabama in Huntsville, pp. 325-355, 1972.
5. H. D. Hibbit, P. V. Marcel and J. R. Rice, "Finite element formulation for problems of large strain and large displacements," Int. J. Solids and Struct., Vol. 6, pp. 1069-1086, 1970.
6. J. F. McNamara, "Incremental stiffness method for finite element analysis of the nonlinear dynamic problem," Ph.D. Thesis, Dept. of Engrg., Brown University, 1972.
7. E. Haug and G. H. Powell, "Finite element analysis of nonlinear membrane structures," SEM Report No. 72-7, Dept. of Civil Engrg., Univ. of California, Berkeley, 1972.
8. W. C. Chao and J. N. Reddy, "Analysis of laminated composite shells using a degenerated 3-D element," Int. J. Numer. Meth. Engrg., Vol. 20, pp. 1991-2007, 1984.
9. T. H. H. Pian and Pin Tong, "Variational formulation of finite-displacement analysis," High Speed Computing of Elastic Structures, B. Fraeijji de Veubeke (ed.), University of Liege, Belgium, pp. 43-63, 1971.
10. K. J. Bathe, E. Ramm and E. L. Wilson, "Finite element formulations for large deformation dynamic analysis," Int. J. Numer. Meth. Engrg., Vol. 9, pp. 353-386, 1975.
11. G. Horrigmoe and P. G. Bergan, "Incremental variational principles and finite element models for nonlinear problems," Computer Meth. Appl. Mech. Engrg., Vol. 7, pp. 201-217, 1976.
12. W. E. Haisler, J. A. Stricklin, and F. J. Stebbins, "Development and evaluation of solution procedures for geometrically nonlinear structural analysis," AIAA J., Vol. 10, No. 3, pp. 264-272, 1972.

13. D. P. Mondkar and G. H. Powell, "Finite element analysis of non-linear static and dynamic response," Int. J. Numer. Meth. Engng., Vol. 11, pp. 499-520, 1977.
14. J. N. Reddy, Energy and Variational Methods in Applied Mechanics, John Wiley, New York, 1984.
15. L. E. Malvern, Introduction to the Mechanics of a Continuous Medium, Prentice-Hall, Englewood Cliffs, N.J., 1974.
16. J. N. Reddy, An Introduction to the Finite Element Method, McGraw-Hill, New York, 1984.
17. E. C. Klang and M. W. Hyer, "The stress distribution in pin-loaded orthotropic plates", Report No. CCMS-85-05, Virginia Polytechnic Institute and State University, Blacksburg, VA 24061, June 1985.
18. T. L. Wilkenson, R. E. Rowlands and R. D. Cook, "An incremental finite-element determination of stresses around loaded holes in wood plates", Computers and Structures, Vol. 14, pp. 123-128, 1981.
19. M. U. Rahman, R. E. Rowland, R. D. Cook and T. L. Wilkenson, "An iterative procedure for finite-element stress analysis of frictional contact problems", Computers and Structures, Vol. 18, pp. 947-945, 1984.
20. E. Hinton, F. L. Scott and R. E. Ricketts, "Local least squares smoothing for parabolic isoparametric elements", Int. J. Numer. Meth. Engng., Vol. 9, pp. 235-238, 1979.
21. G. Loubignal, G. Cantin and G. Touzot, "Continuous stress fields in finite element analysis", AIAA J., Vol. 15, pp. 1645-1646, 1977.
22. K. J. Bathe and A. Chaudhary, "A solution method for planar and axisymmetric contact problems", Int. J. Numer. Meth. Engng., Vol. 21, pp. 65-88, 1985.
23. F. A. Mirza and M. D. Olson, "The mixed finite element method in plane elasticity", Int. J. Numer. Meth. Engng., Vol. 15, pp. 273-289, 1980.
24. J. T. Holden, "On the finite deflections of thin beams", Int. J. Solids Struct., Vol. 8, pp. 1051-1055, 1972.

UNCLASSIFIED

SECURITY CLASSIFICATION OF THIS PAGE (When Data Entered)

REPORT DOCUMENTATION PAGE		READ INSTRUCTIONS BEFORE COMPLETING FORM
1. REPORT NUMBER VPI-E-86.2	2. GOVT ACCESSION NO.	3. RECIPIENT'S CATALOG NUMBER
4. TITLE (and Subtitle) A COMPUTATIONAL MODEL FOR CONTACT STRESS PROBLEMS		5. TYPE OF REPORT & PERIOD COVERED Interim
		6. PERFORMING ORG. REPORT NUMBER ONR-MECH-R-2
7. AUTHOR(s) J. N. Reddy and P. R. Heyliger		8. CONTRACT OR GRANT NUMBER(s) N00014-84-K-0552
9. PERFORMING ORGANIZATION NAME AND ADDRESS Virginia Polytechnic Institute and State University Blacksburg, Virginia 24061		10. PROGRAM ELEMENT, PROJECT, TASK AREA & WORK UNIT NUMBERS NR-064-727/5-4-84 (430)
11. CONTROLLING OFFICE NAME AND ADDRESS Office of Naval Research Mechanics Division (Code 430) 800 N. Quincy St., Arlington, VA 22217		12. REPORT DATE January 1986
		13. NUMBER OF PAGES 35
14. MONITORING AGENCY NAME & ADDRESS (if different from Controlling Office)		15. SECURITY CLASS. (of this report) UNCLASSIFIED
		15a. DECLASSIFICATION/DOWNGRADING SCHEDULE
16. DISTRIBUTION STATEMENT (of this Report)  This document has been approved for public release and sale; distribution unlimited.		
17. DISTRIBUTION STATEMENT (of the abstract entered in Block 20, if different from Report)		
18. SUPPLEMENTARY NOTES		
19. KEY WORDS (Continue on reverse side if necessary and identify by block number) Computational model, contact friction, contact stress, finite element model, incremental formulation, mixed formulation, nonlinear analysis, planar contact, updated Lagrangian formulation.		
20. ABSTRACT (Continue on reverse side if necessary and identify by block number) A mixed finite element model based on the incremental, updated Lagrangian, nonlinear description of continua is developed using a mixed virtual work statement, and its application to planar elastic contact problems is discussed. The computational model is evaluated by comparing the numerical results with those obtained by a displacement finite element model. The mixed model, which contains displacements and stresses as nodal degrees of freedom, yields accurate stresses while the displacements are no better than those of the displacement finite element model.		

DD FORM 1473 1 JAN 73 EDITION OF 1 NOV 65 IS OBSOLETE

UNCLASSIFIED

SECURITY CLASSIFICATION OF THIS PAGE (When Data Entered)

END

FILMED

3

-86

DTIC